Cellular-automata studies of circular Couette flows and chaotic mixing

Renata B. Rybka
Department of Physics of Atmosphere, Institute of Geophysics, Polish Academy of Sciences, 01-452 Warsaw, Poland

Marek Cieplak
Institute of Physics, Polish Academy of Sciences, 02-668 Warsaw, Poland

U. D'Ortona and D. Salin
Laboratoire d'Acoustique et Optique de la Matiére Condensèe, Universitè Pierre et Marie Curie, 75252 Paris, France

Jayanth R. Banavar
Department of Physics and Materials Research Laboratory, 104 Davey Laboratory, The Pennsylvania State University, University Park, Pennsylvania 16802
(Received 26 October 1992)

The results of numerical calculations of the velocity profiles and the viscosities of Boolean and Boltzmann cellular automata for circular Couette flows in two dimensions are presented. The necessary forcing rules to induce such flows are constructed. It is shown that the Boltzmann cellular automata offer a more natural way of simulating flows around curved boundaries. A comparison to the results for Poiseuille and planar Couette flows is made. The Boltzmann automata are used to study chaotic mixing in time-periodic flows between two eccentric circles. The Poincaré sections obtained are similar to those found in experiments.

PACS number(s): 05.45.+b, 66.10.Cb

I. INTRODUCTION

Lattice-gas models have been the subject of much research [1,2]. These models are cellular automata consisting of fictitious particles which hop synchronously between sites of a regular lattice and scatter on the sites of the lattice. The rules of behavior of the particles depend on the solutions of which partial differential equation the automaton is supposed to imitate. For applications in hydrodynamics, the collision laws are chosen to satisfy the microscopic conservation laws of mass and momentum. Frisch, Hasslacher, and Pomeau [3] (FHP) have shown that such two-dimensional (2D) cellular automata simulate the behavior characteristic of the 2D Navier-Stokes equations for sufficiently large sizes of cells over which local averages are calculated. Similar methods to study 3D systems have been also developed [1,4].

The cellular automata have been used to study a variety of systems such as two-fluid systems with interfaces [5], viscous fingers [6], systems undergoing the liquid-gas transition [7], suspensions [8], polymers [9], and phenomena of dispersion [10] and diffusion [11].

The cellular automata used in these problems are usually Boolean: discrete velocity states at a site are either occupied or not, as described in Sec. II. Recently automata defined in terms of continuous degrees of freedom have been introduced [12–14]. Their dynamics relates to flows of probabilities and not of actual microscopic configurations. The disadvantage of these so-called Boltzmann automata is that the floating-point algebra involved leads to round-off errors but, on the other hand, no coarse graining is needed and the noise and equilibration times are reduced significantly. In this paper we demonstrate that the Boltzmann automata offer further advantages in studies of flows in confined geometries such as found in porous media where the boundary walls are curved.

In this paper, as a case in point, we discuss a circular Couette flow [15] which is induced by a shear provided by moving walls. The flow is considered to take place between two independently rotating coaxial cylinders, which in the two-dimensional geometry used here are represented by two concentric circles. In order to impart momentum at the walls velocity states of the cellular automata particles have to undergo changes described by certain forcing rules. In Sec. III we construct such forcing rules for the Boolean automata, in Sec. IV we use them to determine velocity profiles and then in Sec. V to calculate viscosity of the system. Comparisons with the planar Couette and the Poiseuille flows are also made here. We find, however, that these rules are quite cumbersome and their generalization would become rather prohibitive in more complicated curved geometries. The forcing rules for the Boltzmann automaton, on the other hand, are very simple and are used in Sec. VI to study chaotic advection in time-periodic circular Couette flows.

The time-periodic flows at low Reynolds numbers result in folding and stretching of a passive tracer leading to a complicated morphology of its distribution. The mixing is chaotic and nonuniform [16–21]. The circular geometry considered in this paper corresponds to the experimentally [22,23] and theoretically [23] studied journal bearing flows. Following our own cellular automata

studies of chaotic mixing in a cavity flow [24] we focus on differences in the mixing morphology in two different realizations of periodic flows: when either one or two walls move at a time. We find that the morphology are reminiscent of those found for the cavity flow mixing. It should be pointed out that the Boltzmann automata define local values of the velocity field without any coarse graining and are thus, also for this reason, ideally suited to studies of chaotic mixing.

II. MODEL

Since the square lattices introduce spurious symmetries [1,3] in the evolution of the fictitious particles, we consider cellular automata on the triangular lattice. All particles have unit mass and are assumed to be either at rest or to move with a unit velocity in one of the six possible directions of the lattice. They are also subject to an exclusion principle—at most only one particle is allowed in any given state (i.e., at a given site having a particular velocity). There are then seven allowed states at each site and the corresponding velocities are

$$\mathbf{C}_0=\mathbf{0}\ , \tag{1}$$

$$\mathbf{C}_\alpha=\left[\cos\left[\frac{\pi}{3}(\alpha-1)\right],\sin\left[\frac{\pi}{3}(\alpha-1)\right]\right]\ ,\quad \alpha=1,\ldots,6\ . \tag{2}$$

In the Boolean case the state of the system is determined by the occupation numbers of the velocity states at all sites. In the Boltzmann approach, on the other hand, the occupation numbers are replaced by corresponding mean population values. Furthermore, one considers evolution not of individual particles but of the whole statistical ensemble of possible trajectories by performing exact enumeration of probabilities. The system is then defined in terms of continuous degrees of freedom which are updated at discrete time steps.

In the starting configuration, we assign randomly on an average ρ_s particles to each site, or equivalently ρ particles per state. The relationship between these two parameters is $\rho_s=(6+n_0)\rho$, where n_0 denotes the number of allowed rest particles at a site.

The lattice gas updating rules consist of two steps: propagation and collision. It is assumed that scattering events take place every time step.

The viscosity of the system depends on what collision rules are allowed in the model. In the Boolean case we use the deterministic collision rules of model FHP II, with $n_0=1$, described in Ref. [1]. These rules take into account certain classes of binary, triple, and ternary collisions and they may generate or remove particles at rest. The identity of the particle is not preserved in the collisions.

For the Boltzmann automata we can easily modify the FHP II collision rules allow for many particles at rest at each site. If n_0 is chosen to satisfy

$$n_0+6=12\frac{1-\rho}{1-2\rho}\ , \tag{3}$$

then the Galilean invariance is introduced into the system [13]. In the studies of chaotic mixing $\rho=\frac{1}{3}$ and $n_0=18$, which satisfies Eq. (3). The Galilean invariance is important in two-fluid flows but in one-fluid flows other choices of n_0, for a given ρ, would also be possible since the velocity field can be rescaled easily.

III. FORCING RULES

Even though our main interest is in the circular flows it is appropriate methodologically to first consider planar flows. We start by identifying the forcing rules which are essential to impose flows in the system.

A. Poiseuille flow

In the case of Poiseuille flow along the y direction, the forcing takes place in the bulk of the system. We now focus on the Boolean automata. Following Ref. [25], we force the flow by adding momentum in the flow direction at a constant rate. A given site allows for acceptance of an external momentum if it has a particle in a state $\alpha=6$ (i.e., in the state with the velocity $\mathbf{C}_6$) and no particle in a state $\alpha=2$, or if it has a particle in a state $\alpha=5$ and no particle in a state $\alpha=3$. A momentum of $\sqrt{3}$ is added to the system if this transfer between the two states takes place. Note that for our flow geometry there are no states with velocities which are parallel to the net flow direction, so there are no single-particle forcing mechanisms allowed.

After each time step, we randomly select a lattice site and, if possible, apply the forcing rule. The forcing process is repeated until the desired amount of momentum has been added. We supplied the system with an average momentum in each time step F equal to 0.76. This effective bulk force, which mimics the pressure gradient, is applied uniformly across the system.

B. Planar Couette flow

In the case of planar Couette flow, there is no bulk forcing and the simulation is more subtle: in addition to the no-slip boundary conditions in the x direction we check whether an extra momentum can be added on impact with the walls. Thus, if a particle in a state $\alpha=3$ impacts on the left-hand side wall ($x=0$) and there is no particle in a state $\alpha=5$ on this site, then the wall imparts $\sqrt{3}$ of momentum by causing the state $\alpha=2$ to be occupied. A similar wall forcing takes place on the right-hand side wall. The wall forcing takes place with a probability p, whenever a possibility for the momentum transfer exists. We studied $p=0.5$ and 1.0. Our results will be shown only for $p=1$ since smaller p's require much longer runs to get a reasonable signal to noise ratio.

C. Circular Couette flow

The microscopic forcing rules are illustrated in Fig. 1. The forcing takes place on a moving circle by adding momentum in the direction tangential to the wall. In Fig. 1 we present all forcing mechanisms, which are operative on the outer circle when it is moving anticlockwise.

There are three main differences from the forcing rules described in Secs. III A and III B.

(i) The amount of momentum added, when pushing, is site dependent.

(ii) The radial and tangential components of the added momentum also depend on the position on the circle.

(iii) The forcing rules may depend not only on the state of the sites under consideration, but also on the state of the neighboring sites.

In the vicinity of the wall there are sites in which only one particle can be directed towards the wall, there are also sites in which up to two, three, or four particles may point towards it. However, it is only when one or two particles are directed towards the moving wall can one add tangential momentum to the system.

Sites in which up to four particles may point towards the wall exist only for a discrete sets of radii R when the centers of the circles reside on a site of the lattice ($n\sqrt{3} \leq R < \sqrt{3n^2+1}$, $n=1,2,\ldots$). We chose the radii of the circles so that there are no such sites in the system.

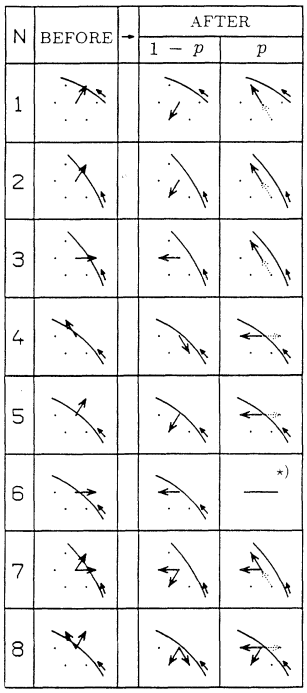

FIG. 1. The microscopic forcing rules for the circular Couette flow as described by the Boolean automata. The rules are operative at the outer circle when it is moving counterclockwise. In the first column are all possible input states with one or two particles impacting on the wall. It is assumed that there are no more particles pointing towards the circle. The possible output states after the impact are shown in the second and third columns. The second column shows the implementation of the no-slip boundary condition. The third column describes the outcome when a relevant forcing rule is applied. The state with a dashed arrow should not be occupied before forcing, if the forcing is to be allowed. The forcing rule is implemented with probability p and the bounce-back condition with probability $1-p$. The situation marked by the asterisk is explained in the text.

In the case of a site in which up to three particles may impact on the wall, and all of the three states are occupied, one can implement only the no-slip boundary conditions.

In the first column of Fig. 1 we show the input states with one or two particles impacting on a moving circle. The possible output states after the impact are shown in the second and third columns. The second column shows implementation of the no-slip boundary condition. The third column describes the outcome when a relevant forcing rule is applied (the state with a dashed arrow should not be occupied before forcing, if the forcing is to be allowed).

Consider, as an example, the first row of the plot. In the input state there is one particle with velocity $\mathbf{C}_2$ and maybe particles with other velocity as well. There are two possible output states after the collision with the wall. One of them is the realization of the no-slip boundary condition (particle with velocity $\mathbf{C}_2$ acquires velocity $\mathbf{C}_5$). The other possibility is the implementation of an appropriate forcing rule, which in this case causes particle in the state $\alpha=2$ to be pushed to the state $\alpha=3$. This forcing rule can be applied only if the $\alpha=3$ state on the neighboring site (the corresponding velocity is shown in dashed line) is unoccupied.

The plots in the sixth row show that in this configuration (marked by the asterisk), there is no new forcing mechanism allowed ($p=0$) because the bounce-back boundary condition automatically imparts a tangential momentum. In general, we permit a particle in a given state to be pushed only to the state nearest the moving circle boundary, which is consistent with the circular flow.

Similar forcing rules are applied to the inner moving circle and to the other rotation direction. The forcing process takes place with a probability p. It is expected that with such forcing rules the added radial momentum averages out to zero and the tangential momentum induces a circular flow.

We carried out simulations for various values of the forcing probability p and found the relation between the velocity v_θ on the moving wall and the pushing rate. The relation is approximately linear as demonstrated in Fig.

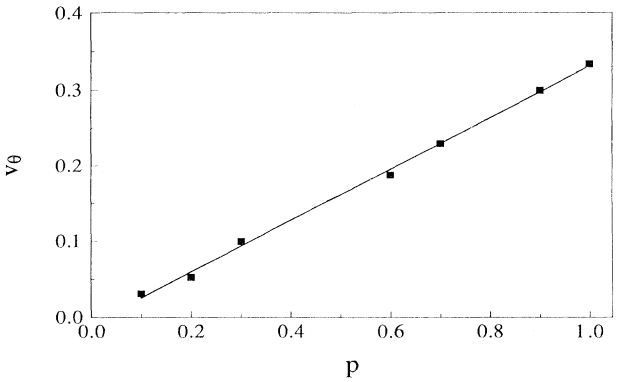

FIG. 2. Tangential velocity v_θ vs the forcing probability p for the circular Couette flow. The site density is $\rho_s=2.1$ and the automaton is Boolean.

2. In order to overcome the noise we choose to do simulations with $p=1$, but even that is not sufficient at higher densities when few channels for pushing are available. For smaller densities, large p means large Reynolds numbers, which may lead to a turbulent flow.

D. Forcing rules for the Boltzmann automata

The implementation of forcing rules at the moving walls consists simply of adding specified contributions to the occupation numbers at the wall sites which would make the boundary flow parallel to the wall. The sizes of the local additive contributions are determined by the magnitude of the wall velocity. Note that in this approach there is no need to monitor instantaneous microscopic conditions at the wall sites.

IV. VELOCITY PROFILES IN THE BOOLEAN AUTOMATA

In the case of Poiseuille and planar Couette flows we take the system to consist of $L\times L$ sites with $L=32$. The linear sizes of the system are then L in the x direction and $L\sqrt{3}/2$ in the direction of the net flow y. For both flows, the boundary conditions in the y direction are chosen to be periodic.

In the case of Poiseuille flow the no-slip boundary conditions are implemented on the wall sites in the x direction by inverting velocities which would carry a particle out of the system (bounce-back boundary condition). We evolve the system for a million (two million for the smallest density) iterations, the first 200 000 (half a million for the lowest density) of which are excluded from the averaging process. The averaging is performed along the lattice lines which are parallel to the walls.

In a 2D Poiseuille flow between two walls there is a mass transport due to a pressure gradient between the ends of the channel. The velocity profile is parabolic and in the continuum limit given by [26]

$$v_y=-\frac{1}{2\eta}\frac{dp}{dy}\left[\frac{h^2}{4}-\left[x-\frac{h}{2}\right]^2\right], \tag{4}$$

where η denotes viscosity and h is the distance between the walls located at $x=0$ and h. The flow is assumed to take place along the y direction and no-slip boundary conditions on the walls are adopted. Kadanoff, McNamara, and Zanetti have demonstrated that lattice-gas automata with suitably chosen bulk forcing rules that push the lattice gas can indeed lead to parabolic profiles and thus allow for the determination of viscosity: a Poiseuille viscometer was constructed.

In the planar Couette flow the velocity profile is linear. In order to determine the viscosity one has to use the defining equation

$$\sigma_{xy}=\eta\frac{dv_y}{dx} \tag{5}$$

and calculate the stress tensor σ_{xy} directly. To this end we need to determine momentum transfer across planes parallel to the walls. In typical numerical calculations the stress tensor is a quantity which is much more noisy than the velocity profiles and its use to calculate viscosity is recommended only under special circumstances such as found in planar Couette flow.

Our studies were carried out for three site densities ρ_s: 1.1, 2.1, and 3.1. As a rule, we found that the smaller the ρ_s the larger the noise. The parabolic and linear flow patterns are found to be very well reproduced by the lattice-gas model for the Poiseuille and planar Couette flows, respectively.

We now turn to the discussion of the circular Couette flows. Similar to the planar Couette flow, there is no overall pressure gradient here and the forcing of the flow takes place not in the bulk but at the walls. In that type of flow the viscosity can be found by determination of the torque (M) acting on the moving circle, which is defined by the equation

$$M=\int_0^{2\pi}\sigma_{r\theta}r^2d\theta\ , \tag{6}$$

where $\sigma_{r\theta}=\eta r[\partial(u_\theta/r)/\partial r]$ and r and θ are the spherical polar coordinates. The viscosity can be then calculated by determining the torque. This should agree with the viscosity obtained either from the velocity profile in the Poiseuille flow or from the stress tensor calculation in any type of flow.

The basic 2D low Reynolds number flow state in the circular Couette case is the one in which the radial component of the velocity is zero and the azimuthal component v_θ is stationary. The distribution of the azimuthal velocity across the annulus is determined by the balance of viscous stresses whereas the pressure distribution is determined by the balance between a radial pressure gradient and the centrifugal force associated with the circular motion. The velocity v_θ depends only on the radial distance r from the axis of symmetry and is given by [15,27]

$$v_\theta=Ar+\frac{B}{r}\ . \tag{7}$$

A and B are constants determined by

$$A=\frac{\Omega_2R_2^2-\Omega_1R_1^2}{R_2^2-R_1^2},\quad B=(\Omega_1-\Omega_2)\frac{R_1^2R_2^2}{R_2^2-R_1^2}\ , \tag{8}$$

where R_1,R_2 are the radii and Ω_1,Ω_2 are the angular velocities of the inner and outer circle, respectively.

The simulations were carried for three cases: the inner circle rotates, but the outer stays at rest; the outer rotates, but the inner stays at rest, and finally both circles rotate, both in the opposite directions. The boundary conditions on the wall at rest are of the no-slip kind whereas on the moving wall forcing rules are implemented as described in Sec. III C. The radii of the smaller and larger cylinders are equal to 30 and 60 lattice constants, respectively. There are of order 10 000 sites between the two circles. There are 414 and 210 sites on the outer and inner walls, respectively.

Some of the flow fields are plotted in Fig. 3. Figures 3(a) and 3(c) were obtained by the Boolean automaton and the maximal forcing probability $p=1$ was used. Figures 3(b) and 3(d) were obtained by the Boltzmann automaton where the tangential addition to the occupation-

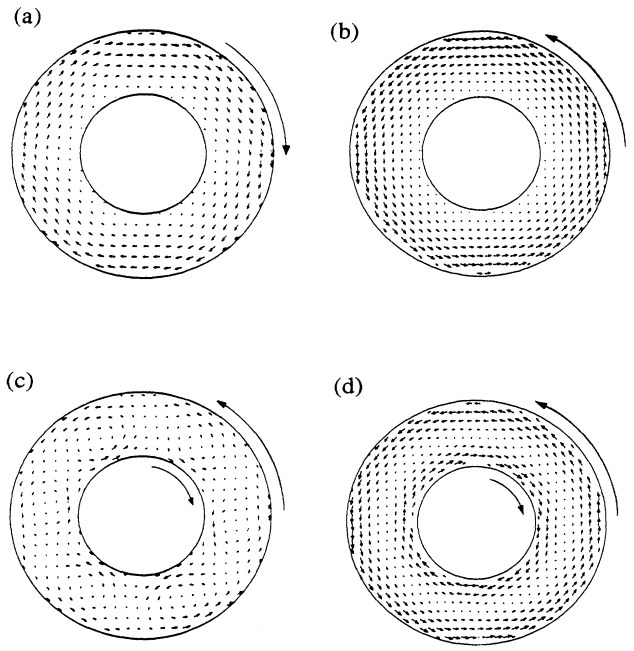

FIG. 3. Flow fields for the circular Couette flow: in the top two figures the inner circle stays at rest and the outer rotates, and in the two bottom figures both circles rotate in opposite directions as indicated by the big arrows. (a) and (c) were obtained by the Boolean automaton ($\rho_s=2.1$) whereas (b) and (d) by the Boltzmann one ($\rho_s=8$). (b) and (d) show local velocities whereas (a) and (c) show coarse-grained velocities (average over 5×5 squares). The "octagonal symmetry" seen in (a) and (c) is just an optical illusion emphasized by the small system size combined with the coarse graining.

al probability of the velocity states was chosen to be equal to 0.1. In the top two figures the inner circle stays at rest and the outer rotates. In Fig. 3(a) the velocity at the moving wall is equal to 0.34 whereas in Fig. 3(b) it is equal to 0.11 [velocity arrows in Figs. 3(b) and 3(d) are magnified by a factor of 3 to be better seen]. In both cases this corresponds to the maximal pushing rates available (in the Boltzmann case the pushing is limited in some states by the occupational probabilities not becoming negative). In the bottom two figures both circles rotate with the same linear velocities as in the corresponding top figures, but in opposite directions. In the Boolean case, especially when both circles are moving, one can see a vortexlike pattern. This is an artifact of the pushing processes being related to the directions available on the triangular lattice. On the other hand, smooth circular velocity fields are observed in the Boltzmann case.

Even though the velocity field obtained by the Boolean automaton is inferior to the one obtained by the Boltzmann automaton, its properties are still quite reasonable, as we shall see in the following. We focus on the velocity field for circular Couette flow in which the inner circle stays at rest and the outer one rotates counterclockwise.

The velocity profiles versus $(r-R_1)/(R_2-R_1)$ are shown in Fig. 4 for three site densities $\rho_s=1.1$, 2.1, and 3.1. Figure 4(a) demonstrates that the radial velocity v_r indeed averages to a value which is close to zero. The root mean square v_r is typically less than 0.01. Figure 4(b) shows the profile of the transverse velocity v_θ. The data points represent values found in the simulations and the lines represent profiles given by Eq. (7), where A and B were calculated from the numerically found Ω_2 at the outer wall. One can see that the best agreement is found for $\rho_s=2.1$. There are at least three sources of the deviations. The first is the possible formation of the Knudsen layer on the wall. The second is the noise, which generates nonzero velocity on the inner resting circle. The lines on Fig. 4(b) were drawn assuming that $\Omega_1=0$. The averaging is performed along coaxial rings of the width of $(R_2-R_1)/7$ (smaller sizes averaging radial bins yielded results, which were too noisy). Finally, one may not be in the low Reynolds number regime. We estimate the Reynolds number to be 45, 27, and 13 for ρ_s equal to 1.1, 2.1, and 3.1. respectively.

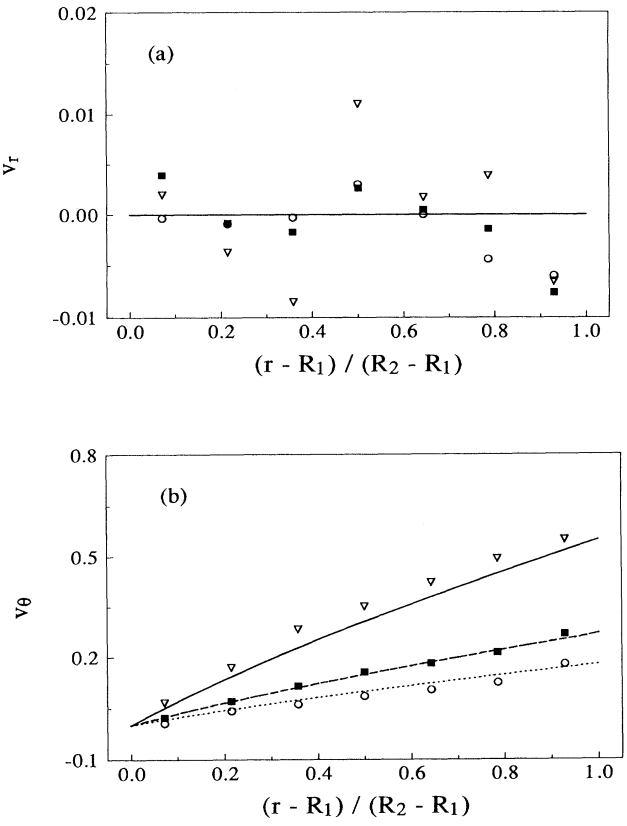

FIG. 4. The velocity profile vs $(r-R_1)/(R_2-R_1)$ for the circular Couette flow in the Boolean automaton. (a) The radial velocity v_r; the line represents a state with a vanishing v_r. (b) The transverse velocity v_θ; the data points correspond to numerically calculated values and the lines represent profiles given by Eq. (7). Triangles denote the site density $\rho_s=1.1$, squares $\rho_s=2.1$, and circles $\rho_s=3.1$.

V. VISCOSITY

A. Boolean automata

The viscosity may be determined in several ways. For both the Poiseuille and planar Couette flows, it may be obtained by dividing the stress tensor by the velocity gradient. This may be done either locally or by fitting the flow profiles and the stress tensor to expected functional forms. In addition, for the Poiseuille flow case, the viscosity may be determined from the velocity profile, by using Eq. (4). The stress tensor is calculated by considering lines parallel to the flow. We determined the y component of the momentum flow from the left end from the right of the plane, similar to the procedure described by Hénon [28]. The quantity is then divided by the length $(L\sqrt{3}/2)$ of the channel. The velocity gradient was calculated by fitting the velocity profile to the expected functional form and taking a derivative.

In the case of Poiseuille flow we fit the velocity profile to a parabola, Eq. (4), assuming a velocity of zero at the walls (even though it is never exactly zero there). The maximum velocity per particle $v_{\max}$ is found for $x=h/2=(L-1)/2$. The pressure gradient in Eq. (4) is replaced by a quantity related to the bulk force

$$\frac{dp}{dy}\simeq\frac{\rho_A F}{\rho_s L(L-\frac{1}{2})}\ , \tag{9}$$

where $\rho_A=\rho_s 2/\sqrt{3}$ is the particle density per unit area. Thus the kinematic viscosity $\nu=\eta/\rho_A$ is given in terms of $v_{\max}$ by

$$\nu=\frac{F}{8v_{\max}\rho_s}\left[\frac{(L-1)^2}{L(L-\frac{1}{2})}\right]\ . \tag{10}$$

In the case of the Poiseuille flow the stress tensor is found to be linear overall. The slope varies with ρ_s in a weak manner. For the planar Couette flow the stress tensor is a constant, but a million time steps were still not sufficient to suppress the noise. The values of the stress tensor, however, are quite reasonable, as seen by the results for the viscosity summarized in Table I.

Consider now the circular Couette flow. A sensible way to calculate viscosity, in this case, is to determine the torque acting on the wall. From Eq. (5) one obtains [15]

$$M=2\pi r^2\left[\eta r\frac{\partial(v_\theta/r)}{\partial r}\right]\Bigg|_{r=R_2}=4\pi\eta B\ , \tag{11}$$

where B is defined in Eq. (8). The torque should be equal to an average force $(\tilde{F})$ acting on the unit length of the outer circle, multiplied by the radius of this circle. The kinematic viscosity, calculated from the torque acting on the outer moving container, is thus given by

$$\nu=\frac{\sqrt{3}}{8\pi}\frac{\tilde{F}R_2}{\rho_s B}\ . \tag{12}$$

The average force $\tilde{F}$ is calculated in the following way. We first sum the tangential momentum transfers at the wall at each instant, averaging the result over time, and divide it by the length of the outer circle $(2\pi R_2)$. Let us denote the result by F'. In order to obtain $\tilde{F}$ we still have to divide F' by the number of outer wall sites per unit length, i.e., $414/2\pi R_2$, and multiply the result by the width of the strip $(R_2-R_1)/7$, which is used in the coarse-graining process. The reason is that the "velocity at the wall" is actually averaged over the width of the strip. We get

$$\tilde{F}=F'\frac{2\pi R_2}{414}\frac{(R_2-R_1)}{7}=3.85F'\ . \tag{13}$$

Thus for $\rho_s=1.1$ we get $\tilde{F}=1.038$ and $B=10.98$; for $\rho_s=2.1$ we get $\tilde{F}=1.248$ and $B=6.68$; and for $\rho_s=3.1$ we get $\tilde{F}=1.016$ and $B=3.56$.

This method of estimating the viscosity is in fact similar to that of calculating the stress tensor, but it is easier to calculate the force acting on the wall than the momentum transfer in a ring across a circular contour. It is evident that for sufficiently large circles this type of flow is equivalent to planar Couette flow.

As seen from Table I all methods of calculating viscosity agree with each other for the particle site density $\rho_s=1.1$, 2.1. In the case of $\rho_s=3.1$ the results are not reliable because the velocity of the outer circle is in that case very small (there are fewer sites at the wall which contain up to two particles) and the signal-to-noise ratio is small. Also, viscosities obtained for situations in which the inner circle is rotating are substantially off the values shown in Table I (e.g., $\nu=0.41$, 0.25, and 0.37 for

TABLE I. Kinematic viscosity for the Poiseuille and planar and circular Couette flows for the three densities considered. In all cases the estimated errors are ±0.03. The data for the circular Couette flow were obtained in the arrangement in which the outer circle rotates and the inner one is held fixed. The fourth column is based on results obtained analytically in Ref. [1] within the lattice Boltzmann approximation. The values from Ref. [1] have been multiplied by $2/\sqrt{3}$. This extra factor compensates for an ambiguity in relating momentum transfers resulting from the forcing rules to real forces and/or pressure gradients. Results obtained in Ref. [13] are almost identical to those shown in the fourth column.

	Poiseuille flow			Planar Couette flow		
ρ_s	Stress tensor	Velocity profile	Ref. [1]	Global	Local	Circular Couette flow
1.1	0.32	0.35	0.34	0.37	0.32	0.36
2.1	0.32	0.34	0.34	0.30	0.31	0.37
3.1	0.56	0.55	0.58	0.55	0.56	

$\rho_s = 1.1$, 2.1, and 3.1, respectively, when the two circles counterrotate). We attribute this to the vortex flow patterns discussed in Sec. IV.

It should be pointed out that the viscosity may also be determined from cellular automata simulations of dynamical approach to steady state. In the planar Couette geometry this has been carried out by Hayot [29]. It would be interesting to study such dynamical effects in cylindrical geometries.

In this paper so far we have learned that the forcing rules needed to induce a circular Couette flow in a Boolean lattice-gas system are possible to construct, but they are rather cumbersome to use. More complex curved flow geometries would need even more elaborate rules. Boltzmann automata, on the other hand, can be forced to flow at moving walls by acquiring a real number shift in the state probabilities at the walls, usually without a necessity to check if some conditions on the states are satisfied or not. Thus in complicated geometries or in the presence of position-dependent bulk forces the flows are described by the Boltzmann algorithms more naturally and these will be used in the next section.

B. Boltzmann automata

The viscosity for the Boltzmann automata can be obtained in a similar way. We used the Poiseuille flow (64×32 sites) and found ν from the velocity profile and from the stress tensor calculations. The two methods agree within the statistical noise and the results are shown in Fig. 5.

The value of ν depends on n_0. For the Galilean invariant case of $n_0 = 18$ and $\rho = \frac{1}{3}$ (i.e., $\rho_s = 8$) we get $\nu = 0.16$. For the same ρ but for $n_0 = 1$ (i.e., $\rho_s = 2.33$) the value of ν is 0.19 (from the velocity profile; 0.20 from the stress tensor), which is of the same order as the Boolean FHP II value. Note, however, that the Boltzmann version of the $n_0 = 1$ automaton has collisions involving the rest particles defined differently than in the Boolean case and the corresponding viscosities should not agree. The difference arises from the fact that in the Boltzmann model collisions involving the rest particles have weights proportional to the number of possible output configurations [13]. This ensures that, in equilibrium, the average ρ in each state at a site is equal. In the Boolean FHP II model, on the other hand, collisions involving rest particles are treated equivalently to other collisions.

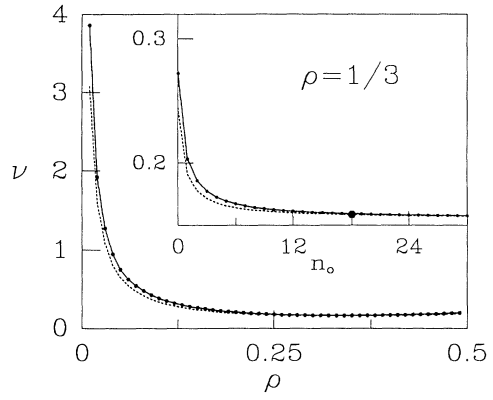

FIG. 5. Kinematic viscosity for the Boltzmann automata obtained from studies of the Poiseuille flow. The figure shows the dependence on ρ, the density per state for those values of ρ and n_0 which satisfy Eq. (3). This is ν found in the Galilean invariant situations. The solid line was obtained from studies of the velocity profile in the Poiseuille flow and the dotted line from the corresponding stress tensor analysis. The inset shows the same quantity, for a fixed $\rho = \frac{1}{3}$, as a function of the number of particles at rest n_0. The Galilean invariant case is marked off by a hexagon.

The main part of Fig. 5 shows ν for n_0 and ρ related by the Galilean invariance condition (3) whereas the inset shows the dependence on n_0 for a fixed ρ.

VI. CHAOTIC MIXING IN JOURNAL-BEARING FLOWS

A study of chaotic mixing of fluids in two-dimensional time-periodic flows serves as a useful model for the understanding of a variety of mixing processes and it provides a visual analog for chaos in area-preserving maps [16–21].

We now focus on 2D mixing processes taking place in flows confined between two eccentric circles [21,23,30]. The main geometrical parameters of this system are the ratio of the radius of the inner circle to the radius of the outer circle $r = R_{\text{in}}/R_{\text{out}}$ and the degree of eccentricity (distance between the centers of the two circles d, normalized by the radius of the outer circle) $\epsilon = d/R_{\text{out}}$. Note that $0 < r + \epsilon < 1$. At low Reynolds numbers the streamlines are determined only be the ratio of angular velocities of the inner and the outer circles $\Omega_{\text{in}}/\Omega_{\text{out}}$. Motivated by the setups of the Swanson-Ottino experiments [23], we choose the following values of the parameters: $R_{\text{in}}/R_{\text{out}} = \frac{1}{3}$, $d/R_{\text{out}} = 0.33$, and $\Omega_{\text{in}}/\Omega_{\text{out}} = -3$. Both the Reynolds number (Re = 16.9) and the Strouhal number are kept low.

We consider the Boltzmann automaton corresponding to $\rho = \frac{1}{3}$ and $n_0 = 18$ and we take $R_{\text{in}} = 10$ and $R_{\text{out}} = 30$. Our simulation are performed for two physical situations.

(a) The moving walls act one at a time. First, the inner circle moves clockwise, for half of the period, and the outer circle stays idle. In the second half of the period the inner circle is idle, but the outer one moves counterclockwise. This is the situation encountered in most of the chaotic flow experiments and is called discontinuous time-periodic flow regime.

(b) The two moving walls act simultaneously. In the first half of the period the inner circle moves clockwise and the outer one moves counterclockwise. In the second half, the directions of the wall motion are reversed. This motion is called continuous time-periodic flow fashion.

In experiments [23] the discontinuous time-periodic protocol [situation (a)] is usually employed, but here we want to compare Poincaré sections and evolutions of blobs of tracers between situations (a) and (b).

Figures 6–8 show the streamlines in the stationary state in the absence of any wall oscillations. In Fig. 6 the outer circle is moving counterclockwise and the inner one

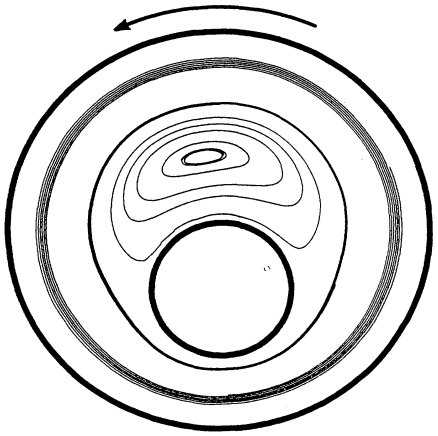

FIG. 6. Streamlines in the stationary state for journal-bearing flow in the case of outer circle moving counterclockwise with the inner one being idle. The Boltzmann automation with $n_0=18$ and $\rho=0.33$ was used here.

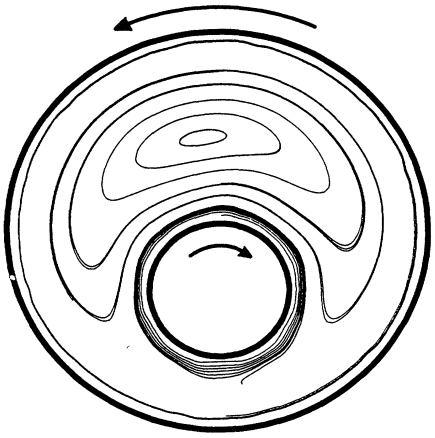

FIG. 8. Same as in Fig. 6 when the inner circle is moving clockwise and the outer one is moving counterclockwise.

stays at rest. In Fig. 7 the situation is reversed and the inner circle is moving clockwise. Figure 8 shows the streamlines in the stationary state for the case of outer circle moving counterclockwise and the inner one clockwise. The lines in Figs. 6–8 show trajectories of a point-like tracer particle placed at various locations of the system. The trajectory of the tracer is determined by the velocity field encountered and is calculated by an interpolation method explained in Ref. [24]. The evolution has been carried out for thousands of steps after reaching the steady flow conditions. Under creeping flow conditions the pattern of the streamlines is determined by the ratio $\Omega_{\text{in}}/\Omega_{\text{out}}$. The ratios corresponding to flows shown in Figs. 6–8 are almost those studied by Ottino [20] in a hydrodynamic model and the similarity of the streamlines to those found by him is very close.

We now consider the time-periodic flows. We have found [24] that the inertial effects (slip time) of regaining stationary state after changing direction of a flow are of the order of 10 time steps, when $n_0=2$. The larger n_0 we are using here slows the dynamics down, but when we deal with flows with long periods T of order of several hundreds or several thousands steps, we can simplify the simulations by working with "photographs" of a stationary velocity field for each half-period instead of actually evolving the cellular automaton system. The automaton is used exclusively to generate the photographs. In scheme (a), for instance, the first photograph has the velocity field corresponding to Fig. 6 whereas the second photograph has the velocity field as in Fig. 7. In order to obtain a truly stationary velocity field we evolve the system for 100 000 time steps. This takes of order 20 h on an IBM486 personal computer. The same number of steps in the Boolean case would take about 9 h.

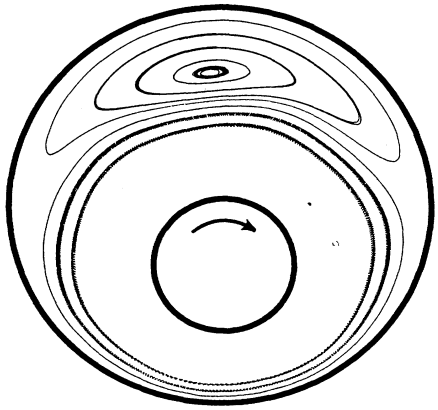

FIG. 7. Same as in Fig. 6 when the inner circle is moving clockwise and the outer one stays idle.

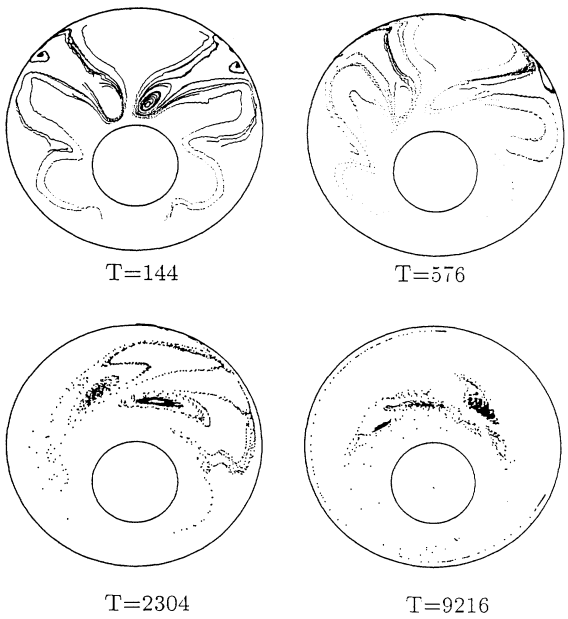

FIG. 9. Poincaré sections for type-A discontinuous flow for four periods 144, 567, 2304, and 9216 as indicated.

FIG. 10. Same as in Fig. 8, but for type-*B* continuous flow.

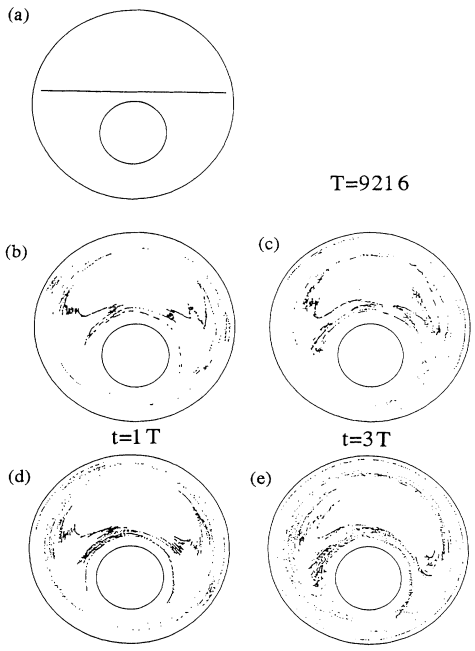

FIG. 11. Trajectories of particles initially located on a horizontal straight line shown in (a). (b) and (d) show positions of the dye particles after time T and $3T$ for situation *A*. (d) and (e) show the corresponding "photographs" for situation *B*.

Poincaré sections show locations of tracer particles every period and they visualize the workings of the mixing process. The Poincaré sections shown in Figs. 9 and 10 were obtained by using 16 tracer particles and evolving their trajectories for 1000 periods. Figure 9 is for situation (a) and Fig. 10 for situation (b). The four values of the periods considered were 144, 576, 2304, and 9216 as indicated (the corresponding Strouhal numbers are 9.47, 2.37, 0.59, and 0.15).

For small periods the flows are not chaotic or only very weakly chaotic and form rolls. The (a)-type flow produces two roll-like structure, whereas the (b)-type flow yields structures which can be thought of as originating from six "vortices." This is reminiscent of the roll structure found in the square cavity flows [24], except that an equivalent of situation (b) produced four rolls, not six. At longer periods rolls cannot be identified and the flows become chaotic. It should be pointed out that the chaotic behavior found here does not originate from any spurious effects due to the cellular automata method: the chaos is observed experimentally and we have attempted to study it within a cellular automaton model.

Finally, we can study mixing of particles arranged initially in some well-defined manner. Figure 11 shows what happens to particles placed along a horizontal line within first three periods in situations (a) and (b), respectively. In both cases $T=9216$. Unlike the square cavity case the mixing in the (a) or (b) way is rather similar, but (b) seems to be more effective.

Our results on the stretching plots and Poincaré sections are qualitatively similar to those found in experiments [21,23,30] They encourage further use of the Boltzmann cellular automata in theoretical studies of such problems. The technique of cellular automata has the advantage of simplicity and computational speed. However, for problems such as one under study, the nontrivial geometry, the need for complex rules, and the long computer runs needed to suppress the noise and obtain an accurate average signal make the Boolean method less competitive. The Boltzmann method saves on averaging, yet may be computationally intensive since no linearization approximation is being made. The Boltzmann method, however, allows for a simple way of accounting for a complicated geometry and makes an alternate viable route of attacking complex hydrodynamic problems such as chaotic mixing.

ACKNOWLEDGMENTS

We thank Daniel Rothman for discussions and for sending us many of his papers and references on cellular automata. We are grateful to Gianluigi Zanetti for useful clarifications of Ref. [25]. We appreciate discussions with Dominique d'Humières and Stephane Zaleski. This work was supported by a grant from the Donors of the Petroleum Research Fund administered by the American Chemical Society, by the U.S.–Polish NSF cooperative grant, by a grant from the Polish Committee of Scientific Research KBN (Grant No. 2-0462-91-01), and by the Center for Academic Computing at Penn State.

[1] U. Frisch, D. d'Humières, B. Hasslacher, P. Lallemand, Y. Pomeau, and J.-P. Rivet, Complex Syst. **1**, 649 (1987).
[2] *Cellular Automata and Modelling of Complex Physical Systems,* edited by P. Manneville, N. Boccara, G. Y. Vichniac, and R. Bideaux (Springer-Verlag, Berlin, 1989).
[3] U. Frisch, B. Hasslacher, and Y. Pomeau, Phys. Rev. Lett. **56**, 1505 (1986).
[4] D. d'Humières, P. Lallemand, and U. Frisch, Europhys. Lett. B **2**, 291 (1986).
[5] D. H. Rothman and J. M. Keller, J. Stat. Phys. **52**, 1119 (1988).
[6] M. Bonetti, A. Noullez, and J.-P. Boon, *Discrete Kinetic Theory, Lattice Gas Dynamics, and Foundations of Hydrodynamics,* edited by R. Monaco (World Scientific, Singapore, 1989), p. 395.
[7] C. Apert and S. Zaleski, Phys. Rev. Lett. **64**, 1 (1990).
[8] A. J. C. Ladd, M. E. Colvin, and D. Frenkel, Phys. Rev. Lett. **60**, 975 (1988).
[9] J. M. Koelman and A. Vianney, Phys. Rev. Lett. **64**, 1915 (1990).
[10] C. Baudet, J. P. Hulin, P. Lallemand, and D. d'Humières, Phys. Fluids A **1**, 507 (1989).
[11] D. Bernardin, O. E. Sero-Guillaume, and C. H. Sun, Physica D **40**, 169 (1991).
[12] G. R. McNamara and G. Zanetti, Phys. Rev. Lett. **61**, 2332 (1988).
[13] A. K. Gunstensen, D. H. Rothman, S. Zaleski, and G. Zanetti, Phys. Rev. A **43**, 4320 (1991).
[14] S. Succi, R. Benzi, and F. Higuera, Physica D **47**, 219 (1991).
[15] D. J. Tritton, *Physical Fluid Dynamics* (Van Nostrand Reinhold, New York, 1977).
[16] H. Aref, J. Fluid. Mech. **143**, 1 (1984).
[17] J. M. Ottino, C. W. Leong, H. Rising, and P. D. Swanson, Nature **333**, 419 (1988).
[18] J. M. Ottino, Sci. Am. **260** (1), 56 (1989).
[19] W. L. Chien, H. Rising, and J. M. Ottino, J. Fluid Mech. **170**, 355 (1986); C. W. Leong and J. M. Ottino, *ibid.* **209**, 463 (1989).
[20] J. M. Ottino, *The Kinematics of Mixing: Stretching, Chaos, and Transport* (Cambridge University Press, Cambridge, 1989).
[21] J. M. Ottino, Phys. Fluids A **3**, 1417 (1991).
[22] J. Chaiken, R. Chevray, M. Tabor, and Q. M. Tan, Proc. R. Soc. London Ser. A **408**, 165 (1986).
[23] P. D. Swanson and J. M. Ottino, J. Fluid Mech. **213**, 227 (1990).
[24] M. Cieplak, U. D'Ortona, D. Salin, R. B. Rybka, and J. R. Banavar, Comp. Mat. Sci. **1**, 87 (1992).
[25] L. P. Kadanoff, G. R. McNamara, and G. Zanetti, Complex Syst. **1**, 791 (1987); Phys. Rev. A **40**, 4527 (1989).
[26] L. D. Landau and E. M. Lifshitz, *Fluid Mechanics* (Addison-Wesley, Reading, MA, 1959).
[27] S. Chandrasekhar, *Hydrodynamic and Hydromagnetic Stability* (Oxford University Press, Oxford, 1961).
[28] M. Hénon, Complex Syst. **1**, 763 (1987).
[29] F. Hayot, Phys. Rev. A **35**, 1774 (1987).
[30] F. J. Muzzio, P. D. Swanson, and J. M. Ottino, Phys. Fluids A **3**, 822 (1991).